Lattice dynamics and dielectric properties of incipient ferroelectric TiO_2 rutile

Changyol Lee
Laboratory of Atomic and Solid State Physics, Cornell University, Ithaca, New York 14853-2501

Philippe Ghosez and Xavier Gonze
Unité de Physico-Chimie et de Physique des Matériaux, Université Catholique de Louvain, B-1348 Louvain-la-Neuve, Belgium

(Received 24 May 1994; revised manuscript received 25 July 1994)

The phonon frequencies at the Γ point, the Born effective charges, and the dielectric permittivity tensors of TiO_2 rutile are calculated using the variational density-functional perturbation theory. The calculated phonon frequencies agree with experiment within a few percent. We analyze the corresponding theoretical eigenvectors as well as the interaction of the vibration modes with the electric field. The Born effective charges of TiO_2 rutile are much larger than the nominal charges of Ti^{4+} and O^{2-} ions, as well as those of SiO_2 stishovite despite the structural similarity. A giant LO-TO splitting is observed for E_u and A_{2u} modes. The O ions in rutile as well as in stishovite are found to have a counterintuitive reversed electronic polarization near the nuclei. The calculated large, anisotropic static dielectric permittivity tensors as well as electronic dielectric permittivity tensors also compare favorably with experiments.

I. INTRODUCTION

TiO_2 has several polymorphs, of which naturally occurring anatase, brookite, and rutile have long been known. Rutile, TiO_2 crystallized in a tetragonal structure that more than 20 other compounds share,[1] is of fundamental and practical interest. Rutile is a wide band-gap semiconductor and is used as a catalyst for chemical reactions. It has some unusual properties.[2–5] The frequency of the soft long-wavelength transverse-optic (TO) A_{2u} mode decreases with decreasing temperature, but never becomes completely soft even at 0 K. Therefore, rutile is classified as an incipient ferroelectric. The A_{2u} mode consists of the displacements of the positively charged Ti ions against negatively charged O ions, along the tetragonal axis. Associated with the soft mode, the static dielectric permittivity tensors have very large values and strong frequency dependencies. Although stishovite, a high-pressure polymorph of SiO_2, has an identical structure, it does not show the unusual behaviors of rutile. These distinct behaviors can be attributed to the fact that Ti in rutile is a transition-metal element with $3d$ electrons, while SiO_2 has only s and p electrons.

The lattice dynamics of solids are intimately related to the thermodynamic properties, the elastic behaviors, and the optical properties. To understand the lattice dynamics of ionic crystals, one should consider the long-range Coulomb interactions between ions, which give rise to the macroscopic electric fields, absent in covalently bonded crystals. There have been theoretical efforts to understand the lattice-dynamical and dielectric properties of rutile using a rigid-ion model and a shell model.[2,4] However, such empirical models show a lack of accuracy and do not provide insight into the relations between the electronic structure and the lattice dynamics.

In this work, we perform a full analysis of the phonon frequencies at the Γ point of the Brillouin zone (BZ), the static and electronic dielectric permittivity tensors, and the Born effective charges of constituent atoms in rutile, from first principles, using a variational approach to density-functional perturbation theory. We also compare the properties of rutile with those of SiO_2 stishovite.[6] The phonon frequencies at the Γ point are accurately calculated, including the soft A_{2u} mode. The Born effective charges of TiO_2 rutile are found to be much larger than the transferred charges in a pure ionic picture, which are +4 for Ti and −2 for O ions. The calculated high-frequency (electronic) dielectric permittivity tensors show reasonable agreement with experiment, as well as the calculated low-frequency (static) dielectric permittivity tensors. We also find the O ions in rutile as well as in stishovite have a counterintuitive reversed electric polarization near the nuclei.

This paper is organized as follows. In Sec. II, we briefly mention our calculational methods. We show our calculated structural parameters, the Born effective charges, the phonon frequencies, the atomic displacement patterns, the oscillator strengths, the change of the electronic density in an electric field, and the dielectric permittivity tensors of TiO_2 in Sec. III. Then, the summary and conclusion are presented in Sec. IV.

II. CALCULATIONAL METHODS

The total energies of the unit cell and the second-order derivatives of the total energies are calculated with the ground-state density-functional theory[7,8] and a variational approach to density-functional perturbation

theory,[9,10] respectively. The variational expressions for the total energies and the second-order derivatives are efficiently evaluated using the conjugate-gradient minimization method.[11,12] Linear response functions such as the phonon frequencies, the dielectric permittivity tensors, the Born effective charges are calculated as second-derivatives of the total energy with respect to atomic displacements or external electrical field. Specifically, the phonon frequencies at wave vector $\mathbf{q}$ are the eigenvalues of the dynamical matrix $D_{\tau_i\sigma_j}(\mathbf{q})$, the second derivative of the total energy with respect to the atomic displacements of atom τ along the i direction and atom σ along the j direction, repeated in each cell with a phase factor $e^{i\mathbf{q}\cdot\mathbf{R}}$, where $\mathbf{R}$ is the position of the cell. $D_{\tau_i\sigma_j}(\mathbf{q})$ is separated into the Ewald part and the electronic part, of which the expression for the Ewald part can be found in Ref. 13, and the electronic part is calculated from

$$E_{\tau_i\sigma_j}(\mathbf{q}) = \sum_{m,\mathbf{k}} sw_{m\mathbf{k}} \Big(\langle u^{\tau_i}_{m\mathbf{k},\mathbf{q}} | H^{(0)}_{\mathbf{k}+\mathbf{q},\mathbf{k}+\mathbf{q}} - \epsilon^{(0)}_{m\mathbf{k}} | u^{\sigma_j}_{m\mathbf{k},\mathbf{q}} \rangle + \langle u^{\tau_i}_{m\mathbf{k},\mathbf{q}} | v^{\sigma_j}_{\mathrm{ext},\mathbf{k}+\mathbf{q},\mathbf{k}} | u^{(0)}_{m\mathbf{k}} \rangle + \langle u^{(0)}_{m\mathbf{k}} | v^{\tau_i}_{\mathrm{ext},\mathbf{k},\mathbf{k}+\mathbf{q}} | u^{\sigma_j}_{m\mathbf{k},\mathbf{q}} \rangle + \langle u^{(0)}_{m\mathbf{k}} | v^{\tau_i\sigma_j}_{\mathrm{ext},\mathbf{k},\mathbf{k}} | u^{(0)}_{m\mathbf{k}} \rangle \Big) + \frac{1}{2} \int \left[\frac{d^2(n\epsilon_{\mathrm{xc}})}{dn^2} \right]_{n=n^{(0)}(\mathbf{r})} (\bar{n}^{\tau_i}_{\mathbf{q}}(\mathbf{r}))^* \bar{n}^{\sigma_j}_{\mathbf{q}}(\mathbf{r}) d\mathbf{r} + 2\pi\Omega_0 \sum_{\mathbf{G}} \frac{(\bar{n}^{\tau_i}_{\mathbf{q}}(\mathbf{G}))^* \bar{n}^{\sigma_j}_{\mathbf{q}}(\mathbf{G})}{|\mathbf{q}+\mathbf{G}|^2} , \tag{1}$$

where the integration and the inner products are over the unit cell volume Ω_0, m and $\mathbf{k}$ run over the occupied states and the BZ, respectively, and $sw_{m\mathbf{k}}$ is the product of the spin degeneracy by the probability of occupancy of state $m,\mathbf{k}$. ϵ_{xc} is the exchange-correlation energy per particle in the local-density approximation (LDA). The definitions of other quantities are as follows: $u^{(0)}_{m\mathbf{k}}$ is the periodic part of the corresponding Bloch wave function and $u^{\tau_i}_{m\mathbf{k},\mathbf{q}}$ is the periodic part of the derivative of the ground-state wave function $u^{(0)}_{m\mathbf{k}}$ with respect to atomic displacements of atom τ along the i direction modulated by the cell phase factor $e^{i\mathbf{q}\cdot\mathbf{R}}$; $H^{(0)}_{\mathbf{k},\mathbf{k}'}$ and $v_{\mathrm{ext},\mathbf{k},\mathbf{k}'}$ are defined by Fourier transformation of unperturbed Hamiltonian $H^{(0)}$ and external potential v_{ext}; $v^{\tau_i}_{\mathrm{ext},\mathbf{k},\mathbf{k}'}$ and $v^{\tau_i\sigma_j}_{\mathrm{ext},\mathbf{k},\mathbf{k}'}$ are the first and second derivative of $v_{\mathrm{ext},\mathbf{k},\mathbf{k}'}$ with respect to atomic displacements of atom τ along the i direction (and atom σ along the j direction); $\bar{n}^{\tau_i}_{\mathbf{q}}(\mathbf{r})$ is the periodic part of the derivative of ground-state electronic density with respect to atomic displacements of atom τ along the i direction modulated by the cell phase factor $e^{i\mathbf{q}\cdot\mathbf{R}}$. $u^{\tau_i}_{m\mathbf{k},\mathbf{q}}$ is obtained by minimizing $E_{\tau_i\tau_i}(\mathbf{q})$ with constraints:

$$\langle u^{\tau_i}_{m\mathbf{k},\mathbf{q}} | u^{(0)}_{m'\mathbf{k}} \rangle = 0 . \tag{2}$$

The electronic dielectric permittivity tensor ϵ_{ij} is obtained from

$$\epsilon_{ij} = \delta_{ij} - \frac{4\pi}{\Omega_0} 2E'_{ij} , \tag{3}$$

where

$$E'_{ij} = \sum_{m,\mathbf{k}} sw_{m\mathbf{k}} \Big(\langle u^{E_i}_{m\mathbf{k}} | H^{(0)}_{\mathbf{k},\mathbf{k}} - \epsilon^{(0)}_{m\mathbf{k}} | u^{E_j}_{m\mathbf{k}} \rangle - i \langle u^{E_i}_{m\mathbf{k}} | u^{k_j}_{m\mathbf{k}} \rangle + i \langle u^{k_i}_{m\mathbf{k}} | u^{E_j}_{m\mathbf{k}} \rangle \Big) + \frac{1}{2} \int \left[\frac{d^2(n\epsilon_{\mathrm{xc}})}{dn^2} \right]_{n=n^{(0)}(\mathbf{r})} [\bar{n}^{E_i}(\mathbf{r})]^* \bar{n}^{E_j}(\mathbf{r}) d\mathbf{r} + 2\pi\Omega_0 \sum_{\mathbf{G}\neq 0} \frac{[\bar{n}^{E_i}(\mathbf{G})]^* \bar{n}^{E_j}(\mathbf{G})}{|\mathbf{G}|^2} . \tag{4}$$

$u^{E_i}_{m\mathbf{k}}$ and $u^{k_i}_{m\mathbf{k}}$ are the derivatives of the ground-state wave function $u^{(0)}_{m\mathbf{k}}$ with respect to an electric field E_i or wave vector k_i, respectively. $u^{E_i}_{m\mathbf{k}}$ can be obtained by minimizing E'_{ii} with the constraints that

$$\langle u^{E_i}_{m\mathbf{k}} | u^{(0)}_{m'\mathbf{k}} \rangle = 0 \tag{5}$$

and $u^{k_i}_{m\mathbf{k}}$ are determined by non-self-consistent minimization of the following expression:

$$E_{\mathrm{NSC}} = \langle u^{k_i}_{m\mathbf{k}} | H^{(0)}_{\mathbf{k},\mathbf{k}} - \epsilon^{(0)}_{m\mathbf{k}} | u^{k_i}_{m\mathbf{k}} \rangle + \langle u^{k_i}_{m\mathbf{k}} | T^{k_i}_{\mathbf{k},\mathbf{k}} - v^{k_i}_{\mathrm{ext},\mathbf{k},\mathbf{k}} | u^{(0)}_{m\mathbf{k}} \rangle + \langle u^{(0)}_{m\mathbf{k}} | T^{k_i}_{\mathbf{k},\mathbf{k}} - v^{k_i}_{\mathrm{ext},\mathbf{k},\mathbf{k}} | u^{k_i}_{m\mathbf{k}} \rangle \tag{6}$$

with the constraints that

$$\langle u^{k_i}_{m\mathbf{k}} | u^{(0)}_{m'\mathbf{k}} \rangle = 0, \tag{7}$$

where $T^{k_i}_{\mathbf{k},\mathbf{k}}$ and $v^{k_i}_{\mathrm{ext},\mathbf{k},\mathbf{k}}$ are the first derivative of kinetic energy operator and external potential with respect to the wave vector k_i.

The Born effective charge tensors $Z^*_{ij,\tau}$ of an atom τ are calculated from the mixed second derivatives of the total energies with respect to the electric field along the i direction and the atomic displacement along the j direction, with

$$Z^*_{ij,\tau} = Z_\tau \delta_{ij} + \Delta Z_{ij,\tau} \ , \tag{8}$$

where Z_τ is the ionic charge of atom τ and $\Delta Z_{ij,\tau}$ is the contribution of electronic screening, which is computed by evaluating the following expression:

$$\Delta Z_{ij,\tau} = 2\Bigg[\sum_{m,\mathbf{k}} sw_{m\mathbf{k}} \left(\langle u^{\tau_j}_{m\mathbf{k},0} | H^{(0)}_{\mathbf{k},\mathbf{k}} - \epsilon^{(0)}_{m\mathbf{k}} | u^{E_i}_{m\mathbf{k}} \rangle - i \langle u^{\tau_j}_{m\mathbf{k},0} | u^{k_i}_{m\mathbf{k}} \rangle + \langle u^{(0)}_{m\mathbf{k}} | \bar{v}^{\tau_j}_{\mathrm{ext},\mathbf{k},\mathbf{k}} | u^{E_i}_{m\mathbf{k}} \rangle \right)$$
$$+ \frac{1}{2} \int \left[\frac{d^2(n\epsilon_{\mathrm{xc}})}{dn^2} \right]_{n=n^{(0)}(\mathbf{r})} [\bar{n}^{\tau_j}_0(\mathbf{r})]^* \bar{n}^{E_i}(\mathbf{r}) d\mathbf{r} + 2\pi\Omega_0 \sum_{\mathbf{G}\neq 0} \frac{[\bar{n}^{\tau_j}_0(\mathbf{G})]^* \bar{n}^{E_i}(\mathbf{G})}{|\mathbf{G}|^2} \Bigg] \ , \tag{9}$$

where $\bar{v}^{\tau_j}_{\mathrm{ext},\mathbf{k},\mathbf{k}}$ is equal to $v^{\tau_j}_{\mathrm{ext},\mathbf{k},\mathbf{k}}$ minus the contribution from $\mathbf{G} = 0$.

Other information on the method and notation can be found in Refs. 9, 10 and 14–16.

The plane-wave basis sets are used to take advantage of the periodicity of the crystal structure. The method adopts the pseudopotential approximation[17,18] to describe the interaction between valence electrons and ionic core. The *ab initio* pseudopotentials for Ti and O atoms are extended norm-conserving and the O pseudopotential is chemical-hardness conserving.[18] Although the Ti pseudopotential has not been built so as to fulfill the condition of the chemical-hardness conservation, $3s$ and $3p$ orbitals are included as semi-core states and provide excellent transferability. Convergence with respect to the plane-wave basis set is achieved with a plane-wave expansion up to the kinetic energy of 45 Ha. A good convergence with respect to the sampling of the Brillouin zone is more difficult to reach. We have used a (4,4,6) Monkhorst-Pack mesh grid for this sampling, estimated to ensure 0.1% relative accuracy on the structural parameters, but could allow a few percent errors on response functions.

These methods, with similar parameters, were applied to various systems such as SiO_2 α-quartz,[9] SiO_2, stishovite[6] $BaTiO_3$,[15] and for the calculation of the effective charges in TiO_2 rutile.[19]

III. RESULTS

A. The structure of rutile

First, we calculate the ground-state structural parameters of rutile. Rutile has a tetragonal unit cell with the symmetry of D^{4h}_{14} in which Ti atoms are at (0,0,0) and $(\frac{1}{2},\frac{1}{2},\frac{1}{2})$ and O atoms are at $(u,u,0)$, $(1-u,1-u,0)$, $(\frac{1}{2}-u,\frac{1}{2}+u,\frac{1}{2})$, and $(\frac{1}{2}+u,\frac{1}{2}-u,\frac{1}{2})$, as shown in Fig. 1. Therefore, the lattice constants a and c and the internal parameter u completely determine the structural degrees of freedom. We calculate the total energies of the unit cell at different lattice constants with optimal internal parameters. The ground-state lattice constants a and c, the internal parameter u are obtained from the minimum-energy configuration. In Table I, we compare our results to experiments and other density-functional-theoretical values. Our calculated structural parameters show good agreement with the experiment and will be used for the following investigations of the response functions.

B. The Born effective charges

The physical meaning of the Born effective charges $Z^*_{ij,\tau}$ is the force in the i direction on the atom τ due to an homogeneous electric field along the j direction, or equivalently, the induced polarization of the solid along the i direction by a unit displacement in the j direction of the atomic sublattice. The effective charges are scalar quantities in a rigid-ion model, but they, in general, have tensorial forms.

Due to the symmetry of the rutile structure, the Born effective charge tensors of the Ti atoms or O atoms in rutile[19] have only three independent components: $Z^*_{xx,\tau}$, $Z^*_{xy,\tau}$, and $Z^*_{zz,\tau}$. $Z^*_{yy,\tau}$ and $Z^*_{yx,\tau}$ are equal to $Z^*_{xx,\tau}$ and $Z^*_{xy,\tau}$, respectively, and other components are zero. In rutile, $Z^*_{ij,\mathrm{Ti}}$=6.338, 0.995, and 7.541 and $Z^*_{ij,\mathrm{O}}$=−3.169, −1.809, and −3.771 for ij=xx, xy, and zz, respectively. Stishovite are found to have $Z^*_{ij,\mathrm{Si}}$=3.803, 0.343, and

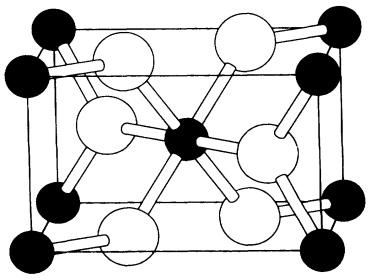

FIG. 1. Unit cell of rutile. Dark and white circles denote Ti and O atoms, respectively. Ti atom at the center of the unit cell with six O atoms shown make up a $TiO_{6/3}$ octahedron. Stishovite has the identical structure with Si atoms at the positions of Ti atoms.

TABLE I. Structural parameters of rutile. Lattice constants a and c are in Å and the unit-cell volume v_0 is in Å^3.

	a	c	v_0	c/a	u
This work	4.536	2.915	59.98	0.643	0.304
Experiment (Ref. 28)	4.5936	2.9587	62.434	0.6441	0.3048
Theory (Ref. 29)	4.567		61.161	0.642	0.305
Theory (Ref. 30)	4.653	2.965	64.84	0.637	0.305
Theory (Ref. 31)	4.584	2.961	62.22	0.646	0.304

4.055 and $Z^*_{ij,\mathrm{O}}$=−1.902, −0.557, and −2.027 in the corresponding order.[6]

When we take a coordinate system whose axes are along the [110], [1$\bar{1}$0], and [001] directions, the Born effective charge tensors are diagonalized, with principal values $\zeta^*_{i,\tau}$. The principal values of the Born effective charges of rutile ($\zeta^*_{i,\mathrm{Ti}}$=7.335, 5.343, and 7.541, and $\zeta^*_{i,\mathrm{O}}$=−4.978, −1.360, and −3.771 for i=1, 2, and 3, respectively) are much larger than those of stishovite ($\zeta^*_{i,\mathrm{Si}}$=4.146, 3.460, and 4.055, and $\zeta^*_{i,\mathrm{O}}$=−2.459, −1.345, and −2.027 for i=1, 2, and 3, respectively). In stishovite, the effective charges are close to the charges in a pure ionic-bond picture, i.e., Si^{4+} and O^{2-}, whereas, in rutile, the effective charges reach up to +7.541 for Ti ions and −4.978 for O ions.

Such anomalous Born effective charges were previously observed in a variety of solids and explained in terms of a bond-orbital model or by a simple tight-binding model.[20,16,21] In a bond-orbital model, the anomalous effective charges can be understood by the dynamical transfer of the charge due to the modification of the bond hybridization during the atomic displacement. That is, when a positive atom is displaced closer to a negative atom, the change in the bond hybridization causes the transfer of electrons from the negative to the positive atoms. When a positive atom moves farther from a negative atom, electrons transfer from the positive to the negative atoms. Therefore, the polarization due to the atomic displacement is dynamically augmented. These effects appear in both rutile and stishovite, as indicated by the differences of the Born effective charges from the charges in a pure ionic-bond picture. The principal value ζ^*_1 is larger than ζ^*_2, because a unit atomic displacement along the bond direction causes more electron transfer than the perpendicular direction. In the simple tight-binding model,[21] the electron transfer is larger in a mixed ionic-covalent bond than a pure covalent or ionic limit.

C. The phonon frequencies at the Γ point

Next, we calculate the phonon frequencies of rutile at the Γ point. The calculated and experimental phonon frequencies are shown in Table II. From the comparison between this work and the known experimental data, one obtains a rms of absolute deviations of 18.7 cm^{-1}, and a rms of relative deviations of 6.0%. The lowest-

TABLE II. The phonon frequencies of rutile and stishovite at the Γ point in cm^{-1}. The first column of experimental data for rutile are inelastic neutron-scattering measurements from Ref. 2 and the second are Raman and infrared measurements from Ref. 32 and 33, respectively. The theoretical values for stishovite are from Ref. 6 and the experimental data are from Ref. 34 for the Raman modes and Ref. 35 for the infrared modes.

	Rutile			Stishovite	
Mode	This work	Experiment		Theory	Experiment
Raman					
B_{1g}	125.2	142	143	214.0	234
E_g	471.5	445	447	585.4	586
A_{1g}	622.5	610	612	754.9	751
B_{2g}	828.0	825	827	954.1	964
Infrared					
E_u (TO)	164.8	189	183	469.0	470
E_u (LO)	351.5	375	373	568.9	565
E_u (TO)	391.3	Not found	388	595.1	580
E_u (LO)	441.7	429	458	705.0	700
E_u (TO)	492.8	494	500	821.6	820
E_u (LO)	808.4	842	807	1043.4	1020
A_{2u} (TO)	176.1	173	167	648.8	650
A_{2u} (LO)	769.3	Not found	812	1048.5	950
Silent					
A_{2g}	415.5	Not found	Silent	599.1	Silent
B_{1u}	116.7	113	Silent	383.6	Silent
B_{1u}	407.5	406	Silent	761.4	Silent

frequency modes contribute the most to the rms error. When the phonon frequencies of rutile and stishovite[6] are compared, the two spectra have similar structure, although a few differences are noticeable: First, the frequencies in stishovite are in general larger than in rutile, due to the lighter Si atom, and secondly, the lower-frequency A_{2u}, E_u, and B_{1u} modes are much softer in rutile than in stishovite. For example, the TO A_{2u} mode has wavelength 176.1 cm^{-1} in rutile and 648.8 cm^{-1} in stishovite. The latter mode is the ferroelectric mode, along the c direction, as we shall see later.

Let us now mention a technical detail, related to the acoustic sum rule and the invariance under translations. Due to the finiteness of our real-space grid ($56 \times 56 \times 36$) for evaluating the exchange-correlation energy, it appears that the translational symmetry of the crystal is sufficiently broken to render the low-frequency modes A_{2u} (176.1 cm^{-1}), B_{1g} (125.2 cm^{-1}), and E_u (164.8 and 351.5 cm^{-1}) of rutile unstable when the phonon frequencies are calculated from the direct diagonalization of the dynamical matrices. This spurious effect can be easily eliminated by projecting out the infinitesimal translation modes off the dynamical matrix, in order to make the acoustic sum rule exactly satisfied. In such a way, we obtain the phonon frequencies listed in Table II. For stishovite, the finiteness of the grid does not have such a drastic effect.

D. Analysis of the eigenvectors

There are 15 optical phonon modes at Γ with symmetry representations A_{1g}, A_{2g}, B_{1g}, B_{2g}, and E_g (Raman-active modes), A_{2u} and E_u (infrared-active modes), and A_{2g} and B_{1u} (optically inactive modes, eventually observed by inelastic neutron-scattering experiments). The E modes are doubly degenerate. The A_{2u} mode and the three doubly degenerate E_u modes exhibit LO-TO splittings. The eigenmodes can also be classified into modes with atomic motion only along the z direction (E_g, B_{1u}, and A_{2u}) and modes with atomic motion only perpendicular to the z direction (all others). The displacement eigenvectors of all the modes except the E_u ones are directly determined from symmetry consideration and the knowledge of the atomic masses. In Fig. 2, we show the pattern of the atomic displacements for the phonon modes at the Γ point.

The dynamical matrices of the ionic crystals at the Γ point are different depending on the direction along which the wave vector is approaching the Γ point, due to the long-range Coulomb interaction. Therefore, the eigenvectors of the TO modes do not necessarily correspond to the ones of the LO modes. We will see that the eigenvectors of the three doubly degenerate E_u TO modes are not directly related to those of the three E_u LO modes, whereas the eigenvector of the A_{2u} TO mode is identical to that of the A_{2u} LO mode due to the symmetry requirements.

In order to quantify the mixing of modes brought by the Coulomb interaction, we build the overlap matrix $\langle \eta^{\mathrm{TO}} | M | \eta^{\mathrm{LO}} \rangle$ shown in Table III, where $|\eta^{\mathrm{TO,LO}}\rangle$ are the eigenvectors of the TO or LO mode and $M = M_\tau \delta_{\tau\tau'}$ where M_τ is the mass of the atom of species τ. The overlap matrix diagonal elements would be 1 if the eigenvectors of the TO and LO mode were identical. In both rutile and stishovite, the eigenvector of each TO mode overlaps the eigenvectors of all the LO modes. The overlap matrix element between the lowest frequency E_u TO mode and the lowest and medium frequency E_u LO modes are large, 0.600 and 0.750 for rutile and 0.564 and 0.819 for stishovite, respectively. The highest-frequency E_u TO mode overlaps significantly with the lowest- and highest-frequency E_u LO modes with the overlap matrix elements -0.710 and 0.617 for rutile and -0.562 and 0.777 for stishovite, respectively. Therefore, it is difficult to describe the eigenvector of an LO mode in terms of a single eigenvector of a TO mode and small perturbations from other TO modes. This analysis will be refined by the examination of the oscillator strengths in the next subsection.

E. The oscillator strengths

Let us define the mode oscillator strength vector $\mathbf{f}$ with components $f_i = \sum_{\tau,j} Z^*_{ij,\tau} \eta^{\mathrm{TO}}_{j,\tau}$ for $i = 1$, 2, and 3. This vector could be used to predict the LO-TO splitting if the eigenvectors of TO modes were identical to those of LO modes, by the following formula:

$$\omega^2_{\mathrm{LO}} - \omega^2_{\mathrm{TO}} = \frac{4\pi}{\Omega} \frac{\left(\sum_i f_i q_i\right)^2}{\sum_{ij} q_i \epsilon_{ij} q_j} \quad \text{as} \quad \mathbf{q} \to 0 \,, \tag{10}$$

where ϵ_{ij} is the calculated electronic dielectric permittivity tensor and Ω is the volume of the unit cell. Note that the oscillator strength vector is zero for the phonon modes, which do not exhibit the LO-TO splittings.

In rutile, the oscillator strength vectors for the three E_u modes belong to the x-y plane, while for the A_{2u} mode, the vector is along the z axis. Due to the double

TABLE III. The overlap matrix element between the eigenvectors of the TO and LO modes in rutile and stishovite. The E_u modes are ordered in the increasing frequency from the top to the bottom and from the left to the right.

	Rutile			Stishovite		
	E_u (LO)	E_u (LO)	E_u (LO)	E_u (LO)	E_u (LO)	E_u (LO)
E_u (TO)	0.600	0.750	0.276	0.564	0.819	0.109
E_u (TO)	−0.369	0.566	−0.737	−0.605	0.500	−0.620
E_u (TO)	−0.710	0.341	0.617	−0.562	0.283	0.777

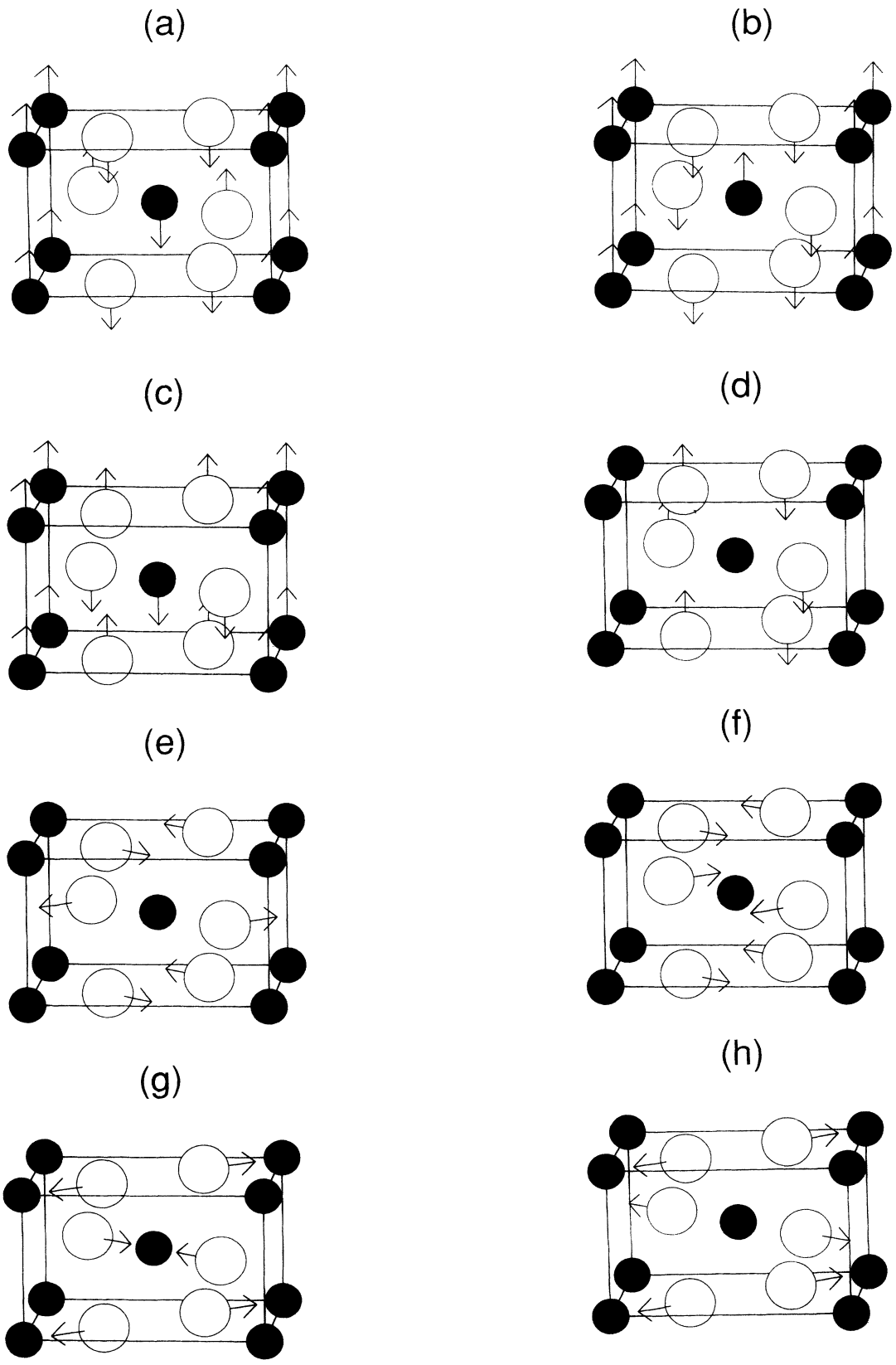

FIG. 2. The atomic displacement pattern for each mode. (a) 116.7-cm^{-1} B_{1u} mode, (b) 176.1-cm^{-1} A_{2u} mode, (c) 407.5-cm^{-1} B_{1u} mode, (d) one of the doubly degenerate 471.5-cm^{-1} E_g modes, (e) 125.2-cm^{-1} B_{1g} mode, (f) 415.5-cm^{-1} A_{2g} mode, (g) 622.5-cm^{-1} A_{1g} mode, (h) 828.0-cm^{-1} B_{2g} mode, (i) one of the doubly degenerate 164.8-cm^{-1} E_u modes, (j) one of the doubly degenerate 391.3-cm^{-1} E_u modes, and (k) one of the doubly degenerate 492.8-cm^{-1} E_u modes.

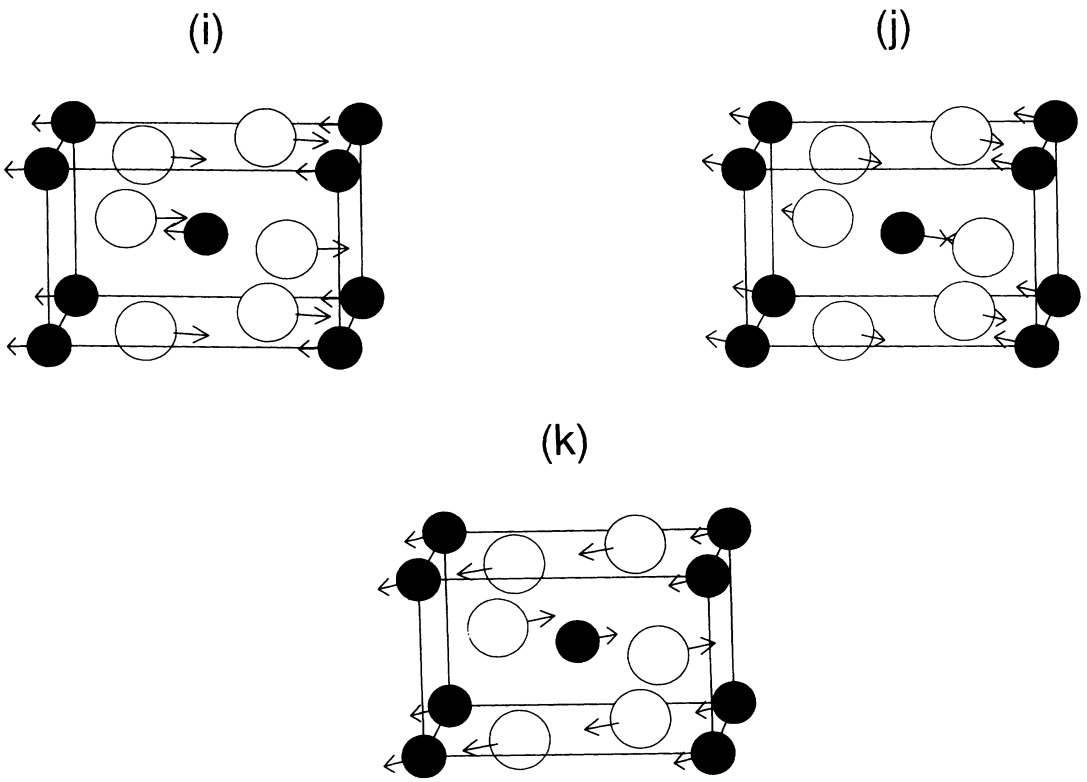

FIG. 2. (*Continued*).

degeneracy of E_u modes, their oscillator strength vector can be rotated in the full x-y plane by unitary transformations, hence we only have to analyze its norm. For the E_u modes with frequency 164.8 cm^{-1}, 391.3 cm^{-1}, and 492.8 cm^{-1}, the oscillator strength norm is 0.0434, 0.0166, and 0.0247 in atomic units, respectively. For the A_{2u} mode, the norm is 0.0570 in atomic units. Using Eq. (10) for predicting the LO frequencies without mode mixing, we obtain 632.6, 456.0, and 603.0 cm^{-1}, respectively. Note that the frequency derived from the smallest-frequency mode is now the largest. Thus, the analysis of the oscillator strengths clarifies the relations between the eigenvectors of the TO and LO modes, in which the lowest-frequency TO E_u mode of rutile couples strongly with the electric field and generates a giant LO-TO splitting.[22] The same phenomenon is also present for the A_{2u} mode also strongly couples with the electric field.

For stishovite, the same analysis gives the following values: for the E_u modes with frequency 469.0 cm^{-1}, 595.1 cm^{-1}, and 821.6 cm^{-1}, the oscillator strength norm is 0.0262, 0.0112, and 0.0172 in the atomic unit, respectively, and the LO frequencies without mode-mixing are 793.1, 654.5, and 922.7 cm^{-1}, respectively. Although less strong than in the case of rutile, the coupling with the electric field is large enough to switch the frequencies of the two lowest modes, already close to each other. For the A_{2u} mode, the norm is 0.0347 in atomic units.

F. The charge-density response to an electric field

Our calculations give us as a byproduct the changes of the electronic density due to the different perturbations. In particular, the effect of an electric field applied upon both rutile and stishovite is shown in Fig. 3. One clearly sees the differences due to the replacement of Ti atoms by Si atoms. There is, moreover, an interesting phenomenon common to both materials. Since the electrons are negatively charged, they are expected to move in a direction opposite to the electric field. However, in the vicinity of the oxygen ions, we can see that the polarization is reversed contrary to the intuition. This phenomenon has also been observed in other oxyde compounds such as α-quartz and $BaTiO_3$. It will be analyzed in more detail for rutile, stishovite, and other materials in an upcoming publication.[23]

G. The dielectric permittivity tensors

Finally, we also present the electronic and static dielectric permittivity tensors. The electronic dielectric permittivity tensors are 7.535 along a axis and 8.665 along c axis. The corresponding experimental values[2] are 6.843 and 8.427, respectively. The discrepancies can be attributed to the well-known LDA underestimation of band gaps as well as the fact that our calculation represents 0

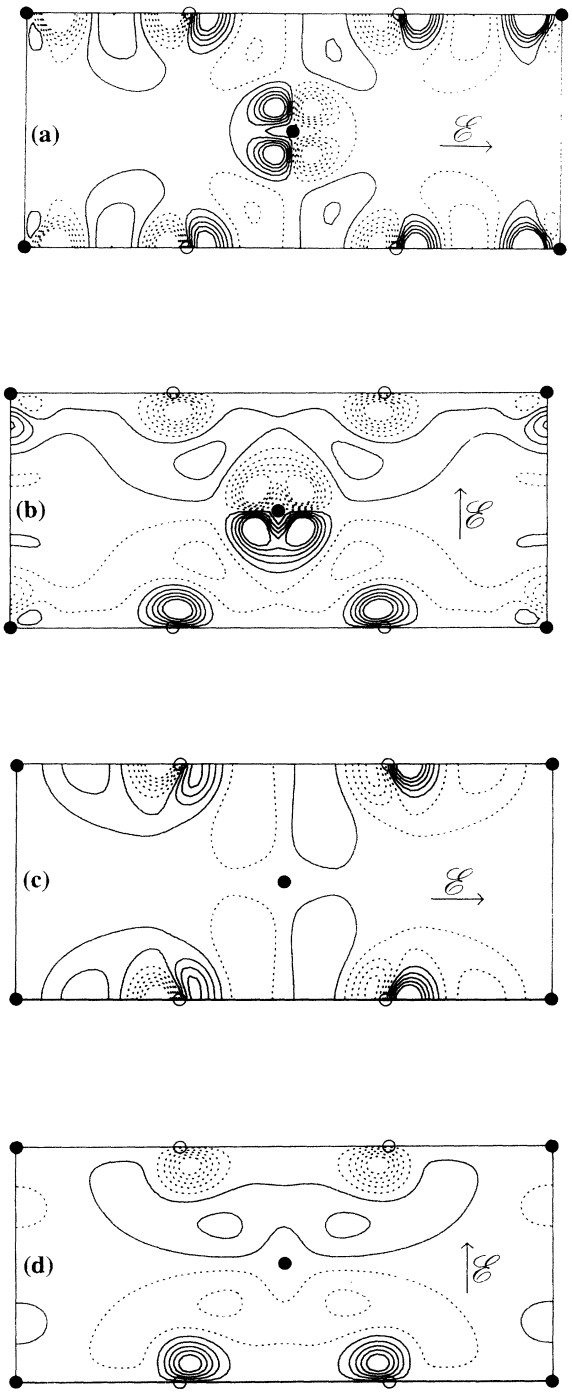

FIG. 3. Changes of the electronic density in TiO_2 and SiO_2 due to an applied electric field, in the linear approximation. Dark and open circles denote Ti (Si) and O atoms, respectively. The cuts are done through a $(1\bar{1}0)$ plane. (a) TiO_2 with a field in the [110] direction, and (b) TiO_2 with a field in the [001] direction, (c) SiO_2 with a field in the [110] direction, and (d) SiO_2 with a field in the [001] direction. The solid isodensity curves correspond to an increase of the electronic density and the dashed isodensity curves to a decrease. The isodensity curves describe changes from -9 electrons/Å^3 to 9 electrons/Å^3, by steps of two electrons/Å^3, for an electric field strength of 10^{10} V/m.

K, while the experiment was done at room temperature. Similar sizes of errors were found in LDA calculations on dielectric permittivity of Si,[24] α-quartz,[9] and stishovite.[6] The calculated electronic dielectric tensors of stishovite are 3.31 and 3.50 along the a and c axis, respectively. Therefore, the ionic polarizabilities in rutile are much larger than those in stishovite.

In order to correct the LDA band gap in calculating the dielectric permittivity tensors, we take advantage of the "scissor correction" technique[25] with a scissor parameter 1.13 eV, the difference from the experimental band gap 3.0 eV (Ref. 26) and our calculated LDA band gap 1.87 eV. The electronic dielectric tensors with the scissor correction are found to be 6.366 and 7.290 along the a and c axis, respectively. The scissor technique brings slightly better agreement for the in-plane dielectric permittivity, but worsens the value along the tetragonal axis. In any case, the anisotropy is not well described.

Without the local-field corrections (and without the scissor correction), the calculated electronic dielectric permittivity tensors would be 7.813 and 8.889 along the a and c axis, respectively. Thus, the local-field effects contribute about 4% in rutile. The local-field effects of a similar size are observed in stishovite.[6]

The static dielectric permittivity tensors using the dynamical matrix and effective charges presented above are calculated to be 117.5 along the a axis and 165.4 along the c axis. These are on the same order of magnitude as the experimentally observed extraordinary large static dielectric permittivity tensors. However, there are discrepancies among the experimental values of the large static dielectric permittivity tensors, i.e., Samara and Peercy[3] report 114.9 along the a axis and 251.0 along the c axis at 4 K, whereas, Parker[27] reports 86 and 170 along the a and c axis, respectively. Stishovite has the calculated static, dielectric permittivity tensors 11.01 along a axis and 9.14 along c axis. The static dielectric permittivity tensors and the frequency of the A_{2u} mode (176.1 cm^{-1}) and one of the TO E_u modes (164.8 cm^{-1}) are related and the softness of these modes in rutile contributes to the exceptional magnitude of the static dielectric permittivity tensor.

IV. CONCLUSION

We have investigated the lattice dynamics and the dielectric properties of TiO_2 rutile and made comparisons with SiO_2 stishovite. The phonon frequencies at the Γ point, the Born effective charges, the static and electronic dielectric permittivity tensors of rutile are calculated using the variational density-functional perturbation theory. The A_{2u} mode in rutile has much lower frequency than that in stishovite. The Born effective charges of rutile are anomalously large and explained in terms of the dynamic electron transfers during atomic displacements. The dynamic electron transfers also occurs in stishovite, although the effects are smaller. We have analyzed in detail the displacement patterns of the different phonon modes at Γ, and have characterized their couplings to the electric field by means of the mode oscil-

lator strength vectors. We obtain an exceptionally high static dielectric permittivity tensors of rutile within the density-functional theory. The electronic dielectric permittivity tensors of rutile are calculated with an error typical of the LDA, when compared with experiment. Surprisingly, the scissor's correction does not lead to better agreement with experiment. Therefore, one could place some doubts about the experimental values. These facts emphasize the importance of the mixed covalent-ionic *s-d* bonding in rutile, related to the large polarizabilities due to the soft A_{2u} and E_u modes, not found in *s-p* bonded stishovite.

ACKNOWLEDGMENTS

We are grateful to Professor M. P. Teter for suggesting the problem. We acknowledge discussions with D. Vanderbilt (who pointed out Ref. 20 to us), R. Resta, and M. Ramamoorthy. This work is supported by the Cornell Theory Center and Corning Incorporated (C.L.), IRSIA-Belgium (P.G.), and FNRS-Belgium (X.G.). Computations were done on IBM RS-6000, at the Laboratory of Atomic and Solid State Physics, Cornell University.

[1] R. W. G. Wyckoff, *Crystal Structures*, 4th ed. (Interscience, New York, 1974).
[2] J. G. Traylor, H. G. Smith, R. M. Nicklow, and M. K. Wilkinson, Phys. Rev. B **3**, 3457 (1971).
[3] G. A. Samara and P. S. Peercy, Phys. Rev. B **7**, 1131 (1973).
[4] F. Gervais and W. Kress, Phys. Rev. B **28**, 2962 (1983).
[5] F. Gervais and B. Piriou, Phys. Rev. B **10**, 1642 (1974).
[6] C. Lee and X. Gonze, Phys. Rev. Lett. **72**, 1686 (1994).
[7] P. Hohenberg and W. Kohn, Phys. Rev. **136**, B864 (1964).
[8] W. Kohn and L. J. Sham, Phys. Rev. **140**, A1133 (1965).
[9] X. Gonze, D. C. Allan, and M. P. Teter, Phys. Rev. Lett. **68**, 3603 (1992).
[10] X. Gonze (unpublished).
[11] M. P. Teter, M. C. Payne, and D. C. Allan, Phys. Rev. B **40**, 12 255 (1989).
[12] M. C. Payne, M. P. Teter, D. C. Allan, T. A. Arias, and J. D. Joannopoulos, Rev. Mod. Phys. **64**, 1045 (1992).
[13] A. A. Maradudin, E. W. Montroll, G. H. Weiss, and I. P. Ipatova, *Theory of Lattice Dynamics in the Harmonic Approximation* in *Solid State Physics*, 2nd ed., edited by H. E. Ehrenreich, F. Seitz, and D. Turnbull (Academic, New York, 1971), Chap. 6.
[14] X. Gonze and J.-P. Vigneron, Phys. Rev. B **39**, 13 120 (1989).
[15] Ph. Ghosez, X. Gonze, and J.-P. Michenaud (unpublished).
[16] Ph. Ghosez, X. Gonze, and J.-P. Michenaud, Proceedings of the 3rd Williamsburg Workshop on First Principles Calculations for Ferroelectrics, Williamsburg, VA, 1993 [Ferroelectrics (to be published)].
[17] W. E. Pickett, Comput. Phys. Rep. **9**, 117 (1989).
[18] M. Teter, Phys. Rev. B **48**, 5031 (1993).
[19] C. Lee and X. Gonze, Phys. Rev. B **49**, 14 730 (1994).
[20] W. A. Harrison, *Electronic Structure and the Properties of Solids* (Dover, New York, 1980).
[21] D. Vanderbilt (unpublished).
[22] W. Zhong, R. D. King-Smith, and D. Vanderbilt, Phys. Rev. Lett. **72**, 3618 (1994).
[23] X. Gonze, Ph. Ghosez, J.-P. Michenaud, and C. Lee (unpublished).
[24] S. Baroni and R. Resta, Phys. Rev. B **33**, 7017 (1986).
[25] Z. H. Levine and D. C. Allan, Phys. Rev. Lett. **63**, 1719 (1989).
[26] J. Pascual, J. Camassel, and H. Mathieu, Phys. Rev. Lett. **39**, 1490 (1977); Phys. Rev. B **18**, 5606 (1978).
[27] R. A. Parker, Phys. Rev. **124**, 1719 (1961).
[28] S. C. Abrahams and J. L. Bernstein, J. Chem. Phys. **55**, 3206 (1971).
[29] M. Ramamoorthy, R. D. King-Smith, and D. Vanderbilt, Phys. Rev. B **49**, 7709 (1994).
[30] K. M. Glassford, N. Troullier, J. L. Martins, and J. R. Chelikowsky, Solid State Commun. **76**, 635 (1990); K. M. Glassford and J. R. Chelikowsky, Phys. Rev. B **45**, 3874 (1992); **46**, 1284 (1992).
[31] D. C. Allan and M. P. Teter, J. Am. Ceram. Soc. **73**, 3247 (1990).
[32] S. P. S. Porto, P. A. Fleury, and T. C. Damen, Phys. Rev. **154**, 522 (1967).
[33] D. M. Eagles, J. Phys. Chem. Solids **25**, 1243 (1964).
[34] M. F. Vigasina, E. V. Guseva, and R. Yu. Orlov, Sov. Phys. Solid State **31**, 747 (1989).
[35] A. M. Hofmeister, J. Xu, and S. Akimoto, Am. Mineral. **75**, 951 (1990).